Olmedo, A., Santiuste, C. & Barbero, E. (2014). An analytical model for predicting the stiffness and strength of pinned-joint composite laminates. *Composites Science and Technology, vol. 90*, pp. 67–73.

DOI: 10.1016/j.compscitech.2013.10.014

An analytical model for predicting the stiffness and strength of pinned-joint composite laminates

A. Olmedo, C. Santiuste, E. Barbero *

Department of Continuum Mechanics and Structural Analysis, University Carlos III of Madrid, Avda de la Universidad 30, 28911 Leganés, Madrid, Spain

A B S T R A C T

An analytical model to predict bearing failure of pinned-joint composite laminates is proposed. The model combines a mass-spring model to reproduce the joint stiffness and a characteristic curve model to predict bearing damage. When bearing failure was verified at any ply, the corresponding spring element was removed from the model. The accuracy of the analytical model was validated through comparison with experimental results. Analytical model predictions agreed with the load–displacement curves and ultrasonic inspections of experimental tests. The present model predicted the different stages in the bearing failure, considering the consecutive failure of the different plies.

Keywords:
A. Laminate
B. Strength
C. Stress concentrations
E. Welding/joining
Analytical model

1. Introduction

Fastener joining is the most widely used method of assembling structural elements in the aerospace industry due to its facility to assemble, disassemble, and repair, as well as its tolerance to environmental effects [1]. Considering that the joints are very often the critical part of a structure, the soundness of their design procedure is reflected on the overall weight, performance and cost of the product. The increased stress-intensity factor at the surrounding of the hole makes the design and assembly process more critical in the case of composite joints than in those based on metallic components [2]. Structural safety needs to be ensured in the aeronautical industry, and therefore the study of mechanical joints in structural composite components has received considerable attention in both the scientific literature and aeronautical standards [3–10].

A major goal of research on the composite bolted joint has been to provide strategies to design composite mechanical joints that avoid catastrophic failure. The basic failure modes in pinned fibre reinforced materials are bearing, net-tension and shear-out failures [3]. From these failure modes only bearing damage causes progressive failure, and thus composite pinned joints are designed to fail under this mode. Bearing failure occurs in the material immediately adjacent to the contacting bolt surface due primarily to compressive stresses [4].

The complex-failure mode of composite bolted joints has been investigated by several researchers in experimental studies, e.g. [5,6]. However, due to the large range of different matrices, fibres, and lay-ups available to the designer, the use of purely empirical design procedures would be prohibitively expensive. It is essential that all the aspects of joint design are well understood, and the development of theoretical reliable models is required to optimise the prediction of composite fastener joints bearing strength.

Due to the complexity of bearing damage, several authors have proposed numerical models to predict composite bolted joint failure but few studies have focused on the development of analytical models. The bearing failure of single-lap bolted joints has been predicted with three-dimensional finite element models, showing good agreement with the experimental data [7–10]. Despite the accuracy of the finite element method [11], the development of simplified models can lead to a better understanding of this phenomenon. Analytical models include the ability to explicitly describe the physical behaviour of fastener joints, and the possibilities for conducting parametric studies. The analyses of the stress field in single-lap bolted joints have revealed that secondary bending causes non-uniform stress distributions throughout the thickness of composite laminates in the vicinity of the bolt hole [12,13], and thus the development of analytical model has been focused on the analysis of pinned joints.

Therefore the analysis of pinned joints has received considerable attention as a preliminary step in the study of composite fastener joints, but also as representative of many assembly configurations [14–16]. The Lekhnitskii method of complex stress function has been extensively used to solve the pin-loaded circular hole problem

* Corresponding author.
E-mail address: ebarbero@ing.uc3m.es (E. Barbero).

in an infinite orthotropic plate. Other works, [17,18], extended this method for arbitrary load direction while considering the presence of friction. Whitworth et al. calculated the characteristic lengths in tension and compression where stresses had to be evaluated to predict bearing failure [19]. These characteristic lengths are a function of mechanical properties and stacking sequence of the laminate. In a later work, Whitworth et al. predicted the bearing failure of pin-loaded composite joints, showing conservative results when joint strength was evaluated as a function of the ratio between plate width and hole diameter [20]. Aluko and Whitworth analysed the effect of the friction coefficient on the stress distribution around the hole boundary for different staking sequences [21].

However, in these works, composite laminates were analysed as a homogeneous anisotropic single layer, and in the present work the Lekhnitskii method was applied to evaluate the failure of each ply. Thus the progressive bearing failure of different plies can be predicted. In addition, the development of a reliable analytical model to predict mechanical behaviour of pinned-joint composite laminates requires the consideration of the joint stiffness and a degradation procedure to reproduce the damage on each ply.

Mass-spring models have been widely used to reproduce the stiffness of fastener joints. Tate and Rosenfeld proposed a mass-spring model to predict the stiffness and the load distribution on bolted-joined isotropic plates [22]. Nelson et al. modified this model to analyse anisotropic composite bolted joints [23]. Recently, McCarthy et al. have developed this model to study the effect of bolt-hole clearance, friction coefficient, and torque level on multi-bolt composite joints [24,25]. Additionally, this model has been modified to predict the through-thickness stiffness in tension-loaded composite bolted joints [26]. The mass-spring models have been applied preferentially to composite bolted joints while considering the equivalent stiffness of the composite plate.

In this work, the McCarthy model was modified to include the consideration of different spring elements to reproduce the stiffness of plies with different orientation. The bearing loads and displacements determined in the mass-spring model were used to evaluate the bearing failure of each ply. When the failure of any ply was verified, the corresponding spring element was removed from the mass-spring model to reproduce the damage. In addition, an experimental test campaign was conducted to validate the analytical model predictions. Force–displacement curves and ultrasonic inspection were used to analyse the bearing failure of pinned-joints on carbon epoxy laminates.

2. Model description

An analytical model to predict bearing failure of composite laminate joints was developed using a pin configuration (Fig. 1a). A tensile load is applied to composite and auxiliary plates, and thus the bearing load is exerted by the cylindrical pin on the composite plate. This problem was modelled in two steps. First, a spring-mass model was developed to reproduce the stiffness of the joint and to calculate the bearing displacement and the bearing load applied on each ply of the laminate. Then, a two-dimensional analysis was performed to calculate the stresses on each ply and to apply a failure criterion to predict the bearing failure.

2.1. Spring-mass model

Fig. 1b illustrates the spring model used to analyse the mechanical behaviour of pinned-joint composite laminates. In this model the following simplifying considerations are assumed:

- The problem is bidimensional; no through-the-thickness variation of the parameters is considered. Therefore, the stacking sequence does not affect the laminate stiffness.
- The friction is neglected.
- The stiffness of each element in the model is lineal.

The particular model shown is for a quasi-isotropic laminate (which includes plies oriented at 0°, 90°, 45°, and −45°). However, the model can be used for any stacking sequence. The pin stiffness, $\boldsymbol{K_{pin}}$, includes the flexibility introduced by shear deformation, $\boldsymbol{K_{pin\text{-}S}}$, and bending moment, $\boldsymbol{K_{pin\text{-}B}}$. The flexibility of the composite plate under bearing loads, $\boldsymbol{K_{be}}$, was represented as three springs in parallel considering the plies with different orientation. The spring, $\boldsymbol{K_{pl}}$, represents the stiffness of the composite plate. The stiffness of the auxiliary plates is considered to be much higher than composite laminate stiffness, and thus it was not included in the model.

Once the stiffness values of all the springs shown in Fig. 2 are known, displacements can be determined for a given force. The equilibrium forces equations for each mass lead to a system of linear equations:

$$[M]\{\ddot{x}\} + [\boldsymbol{K}]\{\boldsymbol{x}\} = \{\boldsymbol{F}\}. \tag{1}$$

For quasi-static conditions the acceleration can be neglected, yielding:

$$[\boldsymbol{K}]\{\boldsymbol{x}\} = \{\boldsymbol{F}\}. \tag{2}$$

Displacement vector, $\{\boldsymbol{x}\}$, can be found by multiplying the load vector, $\{\boldsymbol{F}\}$, by the inverse of stiffness matrix $[\boldsymbol{K}]$. Considering the spring-mass model shown in Fig 2, Eq. (2) yields:

$$\begin{bmatrix} K_{pl} + (K_0 + K_{90} + K_{\pm 45}) & -(K_0 + K_{90} + K_{\pm 45}) & 0 \\ -(K_0 + K_{90} + K_{\pm 45}) & (K_0 + K_{90} + K_{\pm 45}) + \dfrac{K_{pin-S} \cdot K_{pin-B}}{K_{pin-S} + K_{pin-B}} & -\dfrac{K_{pin-S} \cdot K_{pin-B}}{K_{pin-S} + K_{pin-B}} \\ 0 & -\dfrac{K_{pin-S} \cdot K_{pin-B}}{K_{pin-S} + K_{pin-B}} & \dfrac{K_{pin-S} \cdot K_{pin-B}}{K_{pin-S} + K_{pin-B}} \end{bmatrix} \begin{Bmatrix} x_1 \\ x_2 \\ x_3 \end{Bmatrix} = \begin{Bmatrix} 0 \\ 0 \\ F \end{Bmatrix}. \tag{3}$$

The composite plate stiffness can be found considering a composite laminate subjected to a uniform tensile load:

$$K_{pl} = \frac{\boldsymbol{E_{Lc}} \cdot \boldsymbol{W_c} \cdot \boldsymbol{t_c}}{\boldsymbol{p_c} - \boldsymbol{D}/2} \tag{4}$$

where $\boldsymbol{E_{Lc}}$ is the equivalent elasticity modulus in the longitudinal direction, which is calculated using the laminate theory; $\boldsymbol{W_c}$ and $\boldsymbol{t_c}$ are width and thickness of the composite plate, respectively; $\boldsymbol{p_c}$ is the distance between the hole surface and the plate-free end where the load is applied; and $\boldsymbol{D}$ is the hole diameter.

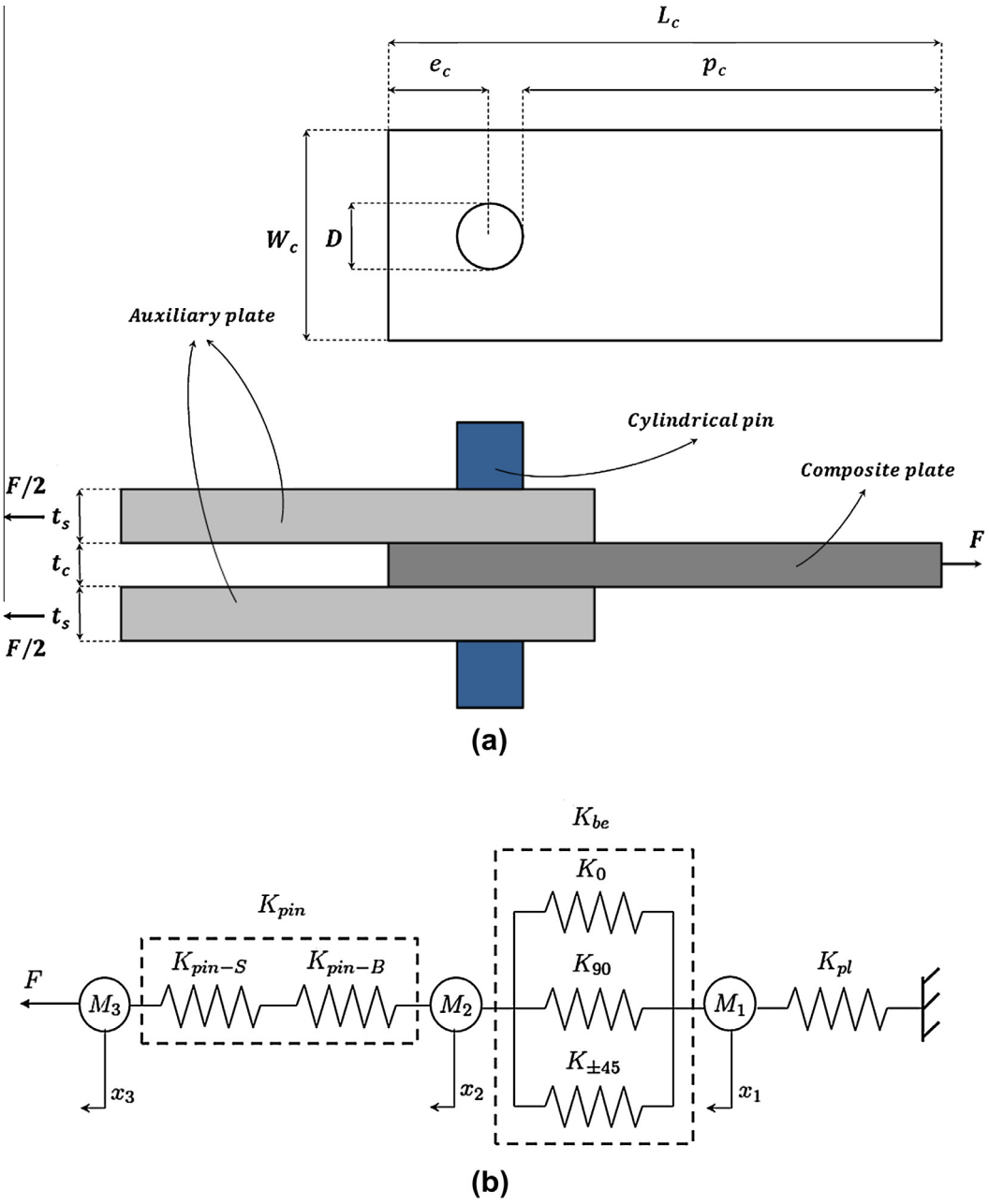

Fig. 1. Schematic representation of the pinned joint: (a) test device used in the pinned-joint tests; (b) spring element model.

The pin stiffness, $\boldsymbol{K_{pin}}$, is calculated considering two springs in a series:

$$\boldsymbol{K_{pin}} = \left[\frac{2 \cdot \boldsymbol{t_s} + t_c}{3 \cdot \boldsymbol{G_b} \cdot \boldsymbol{A_b}} + \frac{\boldsymbol{L_b}^3}{192 \cdot \boldsymbol{E_b} \cdot \boldsymbol{I_b}}\right]^{-1}, \tag{5}$$

where $\boldsymbol{E_b}$ and $\boldsymbol{G_b}$ are Young and shear modulus of the pin material, $\boldsymbol{A_b}$ and $\boldsymbol{I_b}$, are the pin cross-section area and second moment of inertia; $\boldsymbol{t_s}$ is the thickness of the auxiliary plates; and $\boldsymbol{L_b}$ is the shank length.

The bearing stiffness, $\boldsymbol{K_{be}}$, considers three springs in parallel, corresponding to the bearing stiffness values of the plies oriented at 0°, 90°, and ±45°. Plies oriented at 45° and −45° present the same stiffness under longitudinal bearing loads, and thus they were grouped in a single spring. The bearing stiffness of the plies was determined by compressive experimental tests, as shown below. For this model to be applied to a laminate with a different stacking sequence, the bearing stiffness of all the orientations must be included.

$$\boldsymbol{K_{be}} = K_0 + K_{90} + K_{\pm 45} \tag{6}$$

For a given load, this model allows the calculation of the global displacement, the bearing displacement, and the bearing load applied on each ply. Thus, a two-dimensional stress analysis was performed to evaluate the bearing failure on each ply. Once the failure of a ply was verified, the stiffness matrix, Eq. (3), was modified by removing the contribution of the corresponding ply in bearing stiffness, Eq. (6).

2.2. Bearing strength prediction

This section describes the method followed to predict the bearing failure of the plies. For a given bearing displacement, deter-

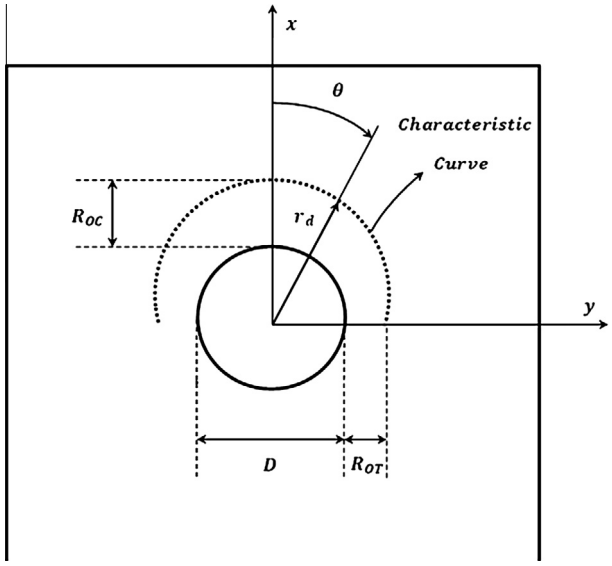

Fig. 2. Composite plate with characteristic curve description.

mined from the spring model, the stress distribution along a characteristic dimension around the hole must first be evaluated at each ply. This characteristic curve around the hole, Fig. 2, indicates the position were bearing failure appears, and thus stresses at characteristic dimensions were used to predict bearing failure.

The characteristic curve model proposed by Chang et al. [27] can be expressed as follows:

$$r_d(\theta) = \frac{D}{2} + \boldsymbol{R_{OT}} + (\boldsymbol{R_{OT}} - \boldsymbol{R_{OC}})\cos\theta \tag{7}$$

where $\boldsymbol{R_{OT}}$ and $\boldsymbol{R_{OC}}$ are the tensile and compressive characteristic lengths. The bearing displacement, $\boldsymbol{x_2} - \boldsymbol{x_1}$, according to springs-mass model, produced at any ply along x axis is denoted by $\boldsymbol{u_0}$. Thus, the boundary condition within the contact region can be expressed as:

$$\boldsymbol{u} = u_0/c \text{ and } \boldsymbol{v} = 0 \quad \text{when } \theta = \pm\frac{\pi}{2} \tag{8}$$

$$\boldsymbol{u} = u_0 \text{ and } \boldsymbol{v} = 0 \quad \text{when } \theta = 0 \tag{9}$$

$$(u_0 - \boldsymbol{u})\cos\theta = \boldsymbol{v}\sin\theta \quad \text{when } -\frac{\pi}{2} \leqslant \theta \leqslant \frac{\pi}{2} \tag{10}$$

$$\sigma_y = 0 \quad \text{when } \theta = \pm\frac{\pi}{2} \tag{11}$$

$$\tau_{xy} = 0 \quad \text{when } \theta = \pm\frac{\pi}{2} \tag{12}$$

where $\boldsymbol{u}$ and $\boldsymbol{v}$ are the displacements along $\boldsymbol{x}$ and $\boldsymbol{y}$ directions, respectively, and $\boldsymbol{c}$ is a constant.

Aluko and Whitworth proposed the following trigonometric series to express displacements $\boldsymbol{u}$ and $\boldsymbol{v}$ along the hole [21]:

$$\boldsymbol{u} = \boldsymbol{U}_1\cos 2\theta + \boldsymbol{U}_2\cos 4\theta \tag{13}$$

$$\boldsymbol{v} = \boldsymbol{V}_1\sin 2\theta + \boldsymbol{V}_2\sin 4\theta, \tag{14}$$

where $\boldsymbol{U_1}$, $\boldsymbol{U_2}$, $\boldsymbol{V_1}$, and $\boldsymbol{V_2}$ are determined by the boundary conditions:

$$\boldsymbol{U}_1 = \frac{c-1}{2c}u_0 \tag{15}$$

$$\boldsymbol{U}_2 = \frac{c+1}{2c}u_0 = V_2 \tag{16}$$

$$\boldsymbol{V}_1 = \left(\frac{c-1}{2c} + \frac{c+1}{c}\right)u_0, \tag{17}$$

In the absence of body forces, the problem of generalized plane stress of a plate reduces to the determination of a stress function on the laminate plane, satisfying these boundary conditions (see [17] for details). Zhang and Ueng showed that the stress functions for an anisotropic plate loaded by a rigid pin with the same diameter as that of the plate hole can be expressed as [18]:

$$\phi_1(z_1) = \boldsymbol{A}^*\ln\zeta_1 + \left(\frac{\boldsymbol{c}-1}{2\boldsymbol{c}}\cdot\frac{q_2 - ip_2}{2\boldsymbol{D}^*} - \frac{\boldsymbol{c}+1}{\boldsymbol{c}}\cdot\frac{ip_2}{2\boldsymbol{D}^*}\right)\frac{u_0}{\zeta_1^2} + \frac{\boldsymbol{c}+1}{2\boldsymbol{c}}\cdot\frac{q_2 - ip_2}{2\boldsymbol{D}^*}\cdot\frac{u_0}{\zeta_1^4} \tag{18}$$

$$\phi_2(z_2) = \boldsymbol{B}^*\ln\zeta_2 + \left(-\frac{\boldsymbol{c}-1}{2\boldsymbol{c}}\cdot\frac{q_1 - ip_1}{2\boldsymbol{D}^*} - \frac{\boldsymbol{c}+1}{\boldsymbol{c}}\cdot\frac{ip_1}{2\boldsymbol{D}^*}\right)\frac{u_0}{\zeta_2^2} - \frac{\boldsymbol{c}+1}{2\boldsymbol{c}}\cdot\frac{q_1 - ip_1}{2\boldsymbol{D}^*}\cdot\frac{u_0}{\zeta_2^4} \tag{19}$$

where $\boldsymbol{A}^*$, $\boldsymbol{B}^*$, $\boldsymbol{D}^*$, $\boldsymbol{p_k}$, and $\boldsymbol{q_k}$ are constants that depend on elastic properties of the lamina [18], $\boldsymbol{i}$ is the imaginary unit, and $\boldsymbol{\xi_k}$, $\boldsymbol{c}$, are defined as a function of the complex roots of the characteristic equation:

$$\zeta_k = \frac{z_k + \sqrt{z_k^2 - R^2(1+\boldsymbol{\mu_k^2})}}{R(1 - i\mu_k)} \tag{20}$$

$$z_k = x + \boldsymbol{\mu_k}y, \quad k = 1,2 \tag{21}$$

$$D^* = \frac{(\mu_1 - \mu_2)\cdot g}{E_x} \tag{22}$$

$$g = \frac{(1 - v_{yx}v_{xy})}{E_y} + \frac{k}{G_{xy}} \tag{23}$$

$$c = \frac{B_{1fr} - A_{1fr}}{A_{1fr}} \tag{24}$$

$$A_{1fr} = (19n + 11nk + 10k - 10v_{yx}) + \boldsymbol{\eta}(11n - 6nk + 15k - 15v_{yx}) \tag{25}$$

$$B_{1fr} = 10n(1-k) + 10\eta(3k - 3v_{yx} + 2nk + n) \tag{26}$$

$$k = -\mu_1\mu_2 = \left(\frac{E_x}{E_y}\right)^{1/2} \tag{27}$$

$$n = -i(\mu_1 + \mu_2) = \left[2(k - v_{yx}) + \frac{E_x}{G_{xy}}\right]^{1/2}, \tag{28}$$

where $\boldsymbol{R}$ is the hole radius, $\boldsymbol{D}^*$ is a parameter that determinates the anisotropy of the lamina, $\boldsymbol{\eta}$ is the friction coefficient, and $\boldsymbol{\mu_k}$ are the complex roots of the characteristic equation:

$$a_{11}\mu^4 + (2a_{12} + a_{66})\cdot\mu^2 + a_{22} = 0. \tag{29}$$

The Lekhnitskii method has been widely used to express the stress field around the hole on pin-loaded anisotropic laminates as a function of the complex roots (29) and the stress functions (18) and (19) [17]. In previous works the anisotropy parameter, $\boldsymbol{D}^*$, was calculated for the whole laminate but in the present model the stress field and the anisotropy parameter were estimated for each ply with different orientations. Evaluation of stresses at all the plies means not only the possibility to be applied to laminates with any staking sequence, but also the ability to reproduce the

consecutive failure of the different laminate plies. The stress distribution around the hole in the laminate plies yields:

$$\sigma_x^j = 2\mathrm{Re}(\mu_1^2\phi_1'(z_1) + \mu_2^2\phi_2'(z_2)) \tag{30}$$

$$\sigma_y^j = 2\mathrm{Re}(\phi_1'(z_1) + \phi_2'(z_2)) \tag{31}$$

$$\tau_{xy}^j = 2\mathrm{Re}(\mu_1\phi_1'(z_1) + \mu_2\phi_2'(z_2)), \tag{32}$$

where $\boldsymbol{j}$ is the ply index. The derivatives of the stress functions (18) and (19) can be introduced into the above equations leading to the following expressions:

$$\sigma_x^j = 2\mathrm{Re}\left\{\left[\frac{A^*}{\zeta_1} - 2\left(\frac{c-1}{2c}\cdot\frac{q_2-ip_2}{2D^*} - \frac{c+1}{c}\cdot\frac{ip_2}{2D^*}\right)\frac{u_0}{\zeta_1^3} - 4\left(\frac{c+1}{2c}\cdot\frac{q_2-ip_2}{2D^*}\right)\frac{u_0}{\zeta_1^5}\right]A_1\mu_1^2 + \left[\frac{B^*}{\zeta_2} - 2\left(-\frac{c-1}{2c}\cdot\frac{q_1-ip_1}{2D^*} + \frac{c+1}{c}\cdot\frac{ip_1}{2D^*}\right)\frac{u_0}{\zeta_2^3} + 4\left(\frac{c+1}{2c}\cdot\frac{q_1-ip_1}{2D^*}\right)\frac{u_0}{\zeta_2^5}\right]A_2\mu_2^2\right\}. \tag{33}$$

$$\sigma_y^j = 2\mathrm{Re}\left\{\left[\frac{A^*}{\zeta_1} - 2\left(\frac{c-1}{2c}\cdot\frac{q_2-ip_2}{2D^*} - \frac{c+1}{c}\cdot\frac{ip_2}{2D^*}\right)\frac{u_0}{\zeta_1^3} - 4\left(\frac{c+1}{2c}\cdot\frac{q_2-ip_2}{2D^*}\right)\frac{u_0}{\zeta_1^5}\right]A_1 + \left[\frac{B^*}{\zeta_2} - 2\left(-\frac{c-1}{2c}\cdot\frac{q_1-ip_1}{2D^*} + \frac{c+1}{c}\cdot\frac{ip_1}{2D^*}\right)\frac{u_0}{\zeta_2^3} + 4\left(\frac{c+1}{2c}\cdot\frac{q_1-ip_1}{2D^*}\right)\frac{u_0}{\zeta_2^5}\right]A_2\right\} \tag{34}$$

$$\tau_{xy}^j = -2\mathrm{Re}\left\{\left[\frac{A^*}{\zeta_1} - 2\left(\frac{c-1}{2c}\cdot\frac{q_2-ip_2}{2D^*} - \frac{c+1}{c}\cdot\frac{ip_2}{2D^*}\right)\frac{u_0}{\zeta_1^3} - 4\left(\frac{c+1}{2c}\cdot\frac{q_2-ip_2}{2D^*}\right)\frac{u_0}{\zeta_1^5}\right]A_1\mu_1 + \left[\frac{B^*}{\zeta_2} - 2\left(-\frac{c-1}{2c}\cdot\frac{q_1-ip_1}{2D^*} + \frac{c+1}{c}\cdot\frac{ip_1}{2D^*}\right)\frac{u_0}{\zeta_2^3} + 4\left(\frac{c+1}{2c}\cdot\frac{q_1-ip_1}{2D^*}\right)\frac{u_0}{\zeta_2^5}\right]A_2\mu_2\right\} \tag{35}$$

where

$$A_k = \frac{\zeta_k}{\sqrt{z_k^2 - R^2(1-\mu_k^2)}}, \quad k = 1,2. \tag{36}$$

Once the stress field is known at the characteristic dimension of each ply, stresses in local axes can be calculated and ply failure can be predicted using an adequate failure criterion. In this work, the Yamada-Sun failure criterion was used [28]. When failure criterion was verified ($e^2 \geqslant 1$) at any ply, the corresponding bearing spring was removed from the mass-spring model to reproduce the ply failure.

$$\left(\frac{\sigma_1}{X_C}\right)^2 + \left(\frac{\tau_{12}}{S_{12}}\right)^2 = e^2 \tag{37}$$

3. Experimental procedure

In this work a laminate made from carbon IM7 fibre and MTM-45-1 epoxy resin with a quasi-isotropic lay-up ($[\pm45/0/90]_{3S}$) was used. Experimental characterization tests according to ASTM D3039M y ASTM D3518M standards were conducted to determine the mechanical properties. Shear modulus and shear stiffness were taken from the literature [29].

Also, the mechanical behaviour under bearing loads was characterized by compression tests on laminates with orientations at 0°, 90°, and ±45°. The specimen dimensions were 200 mm long, 20 mm wide, and 4 mm thick. These rectangular specimens were subjected to a uniform bearing load. The results of the bearing characterization tests were used to determine the value of the bearing stiffness of each ply and the compressive characteristic length ($\boldsymbol{R_{oc}}$). Thus the present approach requires these experimental tests to find the model parameters. The parameters were determined by the characterization tests, and thus the model is a predictive tool that can be used to analyse composite pinned joints with any stacking sequence.

The bearing stiffness of each group of plies ($\boldsymbol{K_0}$, $\boldsymbol{K_{90}}$, and $\boldsymbol{K_{\pm45}}$) was determined as a function of the bearing modulus ($\boldsymbol{E_{be}}$), the hole diameter, the thickness of the plies group ($\boldsymbol{t_j}$) and the characteristic length subjected to bearing stresses ($\boldsymbol{L_0}$):

$$K_j = \boldsymbol{E_{be}^j}\frac{D\cdot\boldsymbol{t_j}}{\boldsymbol{L_0}}. \tag{38}$$

The bearing modulus was calculated as a function of the experimental force–displacement slope ($\boldsymbol{K_{exp}}$), the characteristic length subjected to bearing stresses, and the specimen width ($\boldsymbol{W}$) and thickness ($\boldsymbol{t}$).

$$\boldsymbol{E_{be}^j} = \boldsymbol{K_{exp}^j}\frac{\boldsymbol{L_0}}{\boldsymbol{t}\cdot\boldsymbol{W}}. \tag{39}$$

Substituting Eq. (39) in Eq. (38) and assuming that the characteristic length subjected to bearing stress is the same for characterization compressive tests and pin-loaded tests, it yields:

$$K_j = K_{exp}^j\frac{D\cdot t_j}{W\cdot t} \tag{40}$$

It should be noticed that the bearing stiffness is independent of the characteristic length.

The compressive characteristic length was measured by analysing the post-mortem specimens. The specimen under bearing load failed by a transverse crack which started at a characteristic length that depends on the laminate orientation. The values of compressive characteristic lengths are shown in Table 1. This model considers only compressive bearing failure, so that tensile characteristic length was not considered.

A pin of 6Al4V titanium alloy measuring 4.8 mm in diameter was used in the pin-bearing tests. The properties of this material were taken from the literature [12]. The friction coefficient between the composite plate and the pin surface was 0.114, according to previous research [10]. All material properties used in the model are summarized in Table 1.

Table 1
Material properties of composite material and titanium. Data from experimental tests and literature [15,32].

Carbon epoxy IM7 MTM-45-1	
Longitudinal modulus, E_1 (GPa)	173
Transverse modulus, E_2 (GPa)	7.36
In-plane shear modulus, G_{12} (GPa)	3.89
Major Poisson's ratio, v_{21}	0.33
Longitudinal tensile strength, X_T (MPa)	2998
Longitudinal compressive strength, X_C (MPa)	1414
Transverse tensile strength, Y_T (MPa)	37
Transverse compressive strength, Y_C (MPa)	169
In-plane shear strength, S_{12} (MPa)	120
Stiffness spring 0°, K_0 (KN/m)	4908
Stiffness spring 90°, K_{90} (KN/m)	941
Stiffness spring ±45°, $K_{\pm45}$ (KN/m)	1782
Compressive characteristic length 0°, R_{OC0} (mm)	4.20
Compressive characteristic length 90°, R_{OC90} (mm)	0.20
Compressive characteristic length ±45°, $R_{OC\pm45}$ (mm)	1.21
Ply thickness (mm)	0.125
Titanium 6Al–4V	
Young's modulus, E_b (GPa)	110
Poisson's ratio, v_b	0.29
Yield stress, σ_{yb} (MPa)	1030

A series of pin-bearing ASTM D5961M standard tests were conducted on CFRP laminates with quasi-isotropic stacking sequence ($[\pm 45/0/90]_{3S}$) using a universal test machine (Instron 8516). The geometry of the composite plate and hole diameter were selected to assure that bearing damage would be the main failure mechanism. The test specimen consists of a rectangular plate of length (L_c) equal to 200 mm, width (W_c) 30 mm, and thickness (t_c) 3 mm. The hole was located centrally at 15 mm (distance e_c) from the edge, with a diameter (D) equal to 4.8 mm. The auxiliary-plate thickness (t_s) was 5 mm.

All specimens were loaded at a crosshead speed of 0.2 mm/min to ensure quasi-static conditions. The specimens tested were analysed using non-destructive ultrasonic inspection. C-Scan images obtained with a SONATEST pulse-echo transducer of 2 MHz were used to study the delaminated area.

4. Results and discussion

Fig. 3 shows a typical load–displacement curve found in experimental tests, where three peaks followed by load drops were observed in all the tested specimens. Three different load drops were distinguished, indicating different steps in the bearing failure evolution. To evaluate the evolution of the damage to the composite plate, some tests were conducted at different load levels and the specimens were analysed by non-destructive ultrasonic inspections. C-Scan images are shown in Fig. 3, indicating the corresponding load level.

The first peak load appeared for an average value of 6.39 kN. After the first peak a load drop was detected in all the experimental tests. This load drop corresponds to significant damage caused by bearing failure. Ultrasonic inspections showed a significant increase in delamination damage after the first peak load, as can be seen by comparing Fig. 3b and c. This delamination damage was produced by the propagation of cracks generated by bearing failure. Between the first and second load peaks, the slope of the force–displacement curve was lower than the initial value, indicating a reduction in laminate stiffness. The delamination initiated at the first load peak was propagated during the test, and thus before the second load peak a significant delaminated area appeared (Fig. 3d). The second load peak indicated bearing failure on different laminate plies; subsequently, the slope of the force–displacement curve was again reduced after the second load peak.

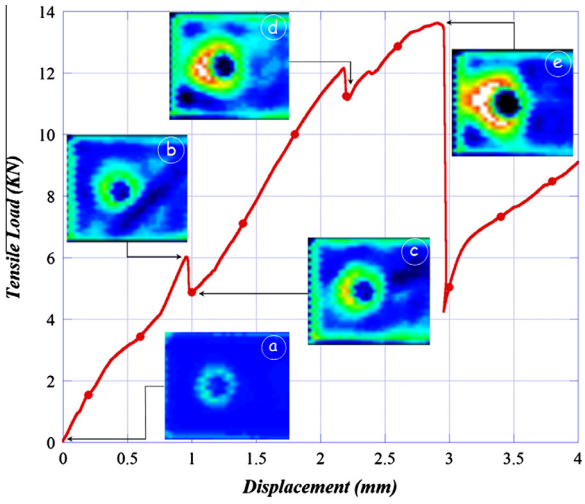

Fig. 3. Experimental load–displacement curve including C-Scan images from ultrasonic inspections.

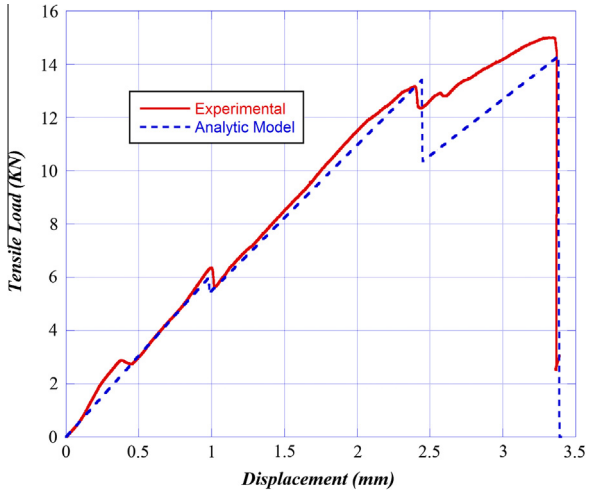

Fig. 4. Load–displacement curve, comparison between analytical model and experimental data.

Finally, a sudden drop occurred after maximum load was reached. This load drop indicated the bearing failure of all the plies.

The mass-springs model was solved by imposing a uniform velocity on the global displacement, $\boldsymbol{X_3}$, to reproduce the experimental control displacement tests. For each incremental displacement, the mass-springs model was used to calculate bearing displacement. Then the bearing failure was evaluated in each ply according to the bearing strength prediction model described in Section 2.2. After bearing failure was verified, the stiffness of the corresponding ply was removed from the spring-mass model for the following increments of displacement. A comparison between the load–displacement curve predicted by the analytical model and the experimental results is shown in Fig. 4.

Analytical model predictions were in excellent agreement with the experimental results. The analytical model was able to predict the progressive failure by bearing load, showing the three peaks observed in the experimental tests. The values of the three peaks were accurately predicted with differences of less than 7%, as shown in Table 2. The initial slope of the force–displacement curve corresponds to the stiffness of the non-damage laminate. According to the analytical model, the first indicates the failure of the plies oriented at 90°. The failure of these plies causes the first drop load and the decrease in the slope of the force–displacement curve. The second peak load is associated with the failure of the plies oriented at ±45°, and therefore the failure of these plies results in a significant drop load and a reduction in the force–displacement curve. Finally, the maximum load indicates the failure of the plies oriented at 0°, and subsequently the failure of the pinned-joint laminate. The reduction of the slope after each ply failure was accurately predicted by the analytical model, as shown in Table 2.

Table 2
Comparison of the model predictions (load slopes and peak loads) with the experimental results.

	First peak	Second peak	Maximum force
Peak loads observed in the load–displacement curve (kN)			
Experimental	6.39 ± 0.32	12.75 ± 0.75	14.22 ± 0.70
Analytic model	5.97	13.41	14.31
Difference (%)	6.5	5.22	0.65
	First slope	Second slope	Third slope
Load–displacement curve slopes (kN/mm)			
Experimental	6.41 ± 0.83	6.20 ± 0.40	3.81 ± 0.22
Analytic model	6.11	5.58	4.13
Difference (%)	4.61	9.93	7.83

Differences between the predictions and the experimental data were less than 10%, and initial stiffness was predicted with an error of less than 5%.

However, there are some discrepancies between the analytical model predictions and the experimental results. The main difference is that the analytical model considered the complete failure of the laminate, when experimental tests showed a sudden drop load followed by a new positive load–displacement slope. Bearing damage is a localized mode of failure; hence, after the surface around the hole is damaged, there is an increment of the pin displacement up to the contact with a new composite surface. Nevertheless, the main objective of the analytical model was to provide an efficient way to predict bearing failure and the stiffness of pinned-joint composite laminates. To prevent the failure of these joints, the design load must be lower than the load necessary to reach the first peak load because, as was shown in Fig. 3, the damage begins at the first peak.

5. Conclusions

An analytical model has been developed to predict the progressive bearing failure of pin-loaded composite laminates. The present model combines a spring-mass model to reproduce the stiffness of the composite pinned-joint and a two-dimensional stress analysis to predict the bearing failure. This can be used to analyse pin-joined laminates with any stacking sequence.

The inclusion of different spring elements reproducing the bearing stiffness of all the plies was necessary to calculate the bearing load and to predict the bearing failure on each ply. Bearing displacement determined with the spring-mass model was used to calculate the stress field at a characteristic dimension. The independent analysis of stress field and failure criterion at plies with different orientation was included to predict the consecutive bearing failure of all the layers.

The proposed model reproduced the different stages in the progressive bearing failure in excellent agreement with the experimental data. The present model provides an accurate method to predict bearing failure of a composite laminate under a pinned-joint configuration. The error in predicting initial stiffness was less than 5%, and the first peak load was predicted with an error of less than 7%. Thus this model can be used as a predictive tool in the design of pinned-joint composite laminates. The understanding of this failure can be used to develop future models in order to predict the bearing failure of other fastener joint configurations such as single-lap bolted joints.

Acknowledgements

The authors are indebted for the financial support of this work to the Ministry of Science and Innovation of Spain (Projects TRA2010_19573 and DPI2010-15123).

References

[1] Camanho PP, Matthews FL. A progressive damage model for mechanically fastened joints in composite laminates. J Compos Mater 1999;33(24):2248–80.
[2] Santiuste C, Olmedo A, Soldani X, Miguélez MH. Delamination prediction in orthogonal machining of carbon long fiber-reinforced polymer composites. J Reinf Plast Compos 2012;31(13):875–85.
[3] Catalanotti G, Camanho PP. A semi-analytical method to predict net-tension failure of mechanically fastened joints in composite laminates. Compos Sci Technol 2013;76:69–76.
[4] Liu F, Zhao L, Mehmood S, Zhang J, Fei B. A modified failure envelope method for failure prediction of multi-bolt composite joints. Compos Sci Technol 2013;83:54–63.
[5] Ireman T, Ranvik T, Eriksson I. On damage development in mechanically fastened composite laminates. Compos Struct 2000;49(2):151–71.
[6] Tong L. Bearing failure of composite bolted joints with non-uniform bolt-to-washer clearance. Composites Part A 2000;31(6):609–15.
[7] Xiao Y, Ishikawa T. Bearing strength and failure behaviour of bolted composite joints (part II: modelling and simulation). Compos Sci Technol 2005;65(7–8):1032–43.
[8] Santiuste C, Barbero E, Miguelez MH. Computational analysis of temperature effect in composite bolted joints for aeronautical applications. J Reinf Plast Compos 2011;30(1):3–11.
[9] Gray PJ, McCarthy CT. A highly efficient user-defined finite element for load distribution analysis of large-scale bolted composite structures. Compos Sci Technol 2011;71(12):1517–27.
[10] Olmedo A, Santiuste C. On the prediction of bolted single-lap composite joints. Compos Struct 2012;94(6):2110–7.
[11] Santiuste C, Sanchez-Saez S, Barbero E. A comparison of progressive-failure criteria in the prediction of the dynamic bending failure of composite laminated beams. Compos Struct 2010;92(10):2406–14.
[12] Ireman T. Three-dimensional stress analysis of bolted single-lap composite joints. Compos Struct 1998;43(3):195–216.
[13] Egan B, McCarthy CT, McCarthy MA, Frizzell RF. Stress analysis of single-bolt, single-lap, countersunk composite joints with variable bolt-hole clearance. Compos Struct 2012;94(3):1038–51.
[14] Mottram, JT, Zafari B. Pin-bearing strengths for bolted connections in fibre-reinforced polymer structures, vol. 64(5). In: Proceedings of 4th Biennial Conference on Advanced Composites in Construction (ACIC) Edinburgh, SCOTLAND; 2011. p. 291–305.
[15] Atas A, Mohamed GF, Soutis C. Modelling delamination onset and growth in pin loaded composite laminates. Compos Sci Technol 2012;72(10):1096–101.
[16] Khashaba UA, Sebaey TA, Alnefaie KA. Failure and reliability analysis of pinned-joints composite laminates: effects of stacking sequences. Composites Part B 2012;45(1):1694–703.
[17] Lekhnitskii SG. Anisotropic plates, English ed. (Tsai SW, Cheron T). London, Gordon and Beach; 1968.
[18] Zhang K, Ueng CES. Stresses around a pin-loaded hole in orthotropic plates. J Compos Mater 1984;18(5):432–46.
[19] Whitworth HA, Othieno M, Barton O. Failure analysis of composite pin loaded joints. Compos Struct 2003;59(2):261–6.
[20] Whitworth HA, Aluko O, Tomilson NA. Application of the point stress criterion to the failure of composite pinned joints. Eng Frac Mech 2008;75(7):1829–39.
[21] Aluko O, Whitworth HA. Analysis of stress distribution around pin loaded holes in orthotropic plates. Compos Struct 2008;86(4):308–13.
[22] Tate MB, Rosenfeld SJ. Preliminary investigation of the loads carried by individual bolts in bolted joints. NACA TN 1051; 1946.
[23] Nelson WD, Bunin BL, Hart-Smith LJ. Critical joints in large composite aircraft structure. NASA CR-3710; 1983.
[24] McCarthy MA, McCarthy CT, Padhi GS. A simple method for determining the effects of bolt–hole clearance on load distribution in single-column multi-bolt composite joints. Compos Struct 2006;73(1):78–87.
[25] McCarthy CT, Gray PJ. An analytical model for the prediction of load distribution in highly torqued multi-bolt composite joints. Compos Struct 2011;93(2):287–98.
[26] Gray PJ, McCarthy CT. An analytical model for the prediction of through-thickness stiffness in tension-loaded composite bolted joints. Compos Struct 2012;94(8):2450–9.
[27] Chang FK, Scott RA, Springer GS. Strength of mechanically fastened composite joints. J Compos Mater 1982;16(6):470–94.
[28] Yamada SE, Sun CT. Analysis of laminate strength and its distribution. J Compos Mater 1978;12(3):275–84.
[29] Ridgard C. Complex Structures for manned/unmanned aerial vehicles. Low Temp Composite Processing Mechanical Property Data. Air Force Research Laboratory. AFRL-RX-WP-TM-2008-4054; 2008.